Marine Structures 65 (2019) 343–361

Contents lists available at ScienceDirect

Marine Structures

journal homepage: www.elsevier.com/locate/marstruc

Experimental and numerical analyses on the dynamic response of aluminum foam core sandwich panels subjected to localized air blast loading

Ganchao Chen[a], Pan Zhang[a,b,c], Jun Liu[a,b,c,*], Yuansheng Cheng[a,b,c], Hao Wang[d]

[a] School of Naval Architecture and Ocean Engineering, Huazhong University of Science and Technology, Wuhan, 430074, PR China
[b] Collaborative Innovation Center for Advanced Ship and Deep-Sea Exploration (CISSE), Shanghai, 200240, China
[c] Hubei Key Laboratory of Naval Architecture and Ocean Engineering Hydrodynamic (HUST), Wuhan, 430074, China
[d] China Institute of Marine Technology & Economic (CIMTEC), Peking, China

ARTICLE INFO

Keywords:
Sandwich structure
Aluminum foam core
Blast loading
Dynamic response

ABSTRACT

This paper presents experimental and numerical investigations into dynamic responses of aluminum foam core sandwich panels subjected to localized air blast loading. It mainly focused on the effects of face-sheet thickness and mass allocation on the deformation responses and energy absorption characteristics. The specimens considered experienced several deformation/failure modes, including localized deformation of front face, large inelastic deformation of back face, core densification and fragmentation and debonding failure. Experimental results show that both the deformation/failure modes and permanent deformation are more sensitive to the variation of front face thickness relative to the one of back face thickness. The optimal mass allocation strategies for the reduction of deformation response are to distribute more mass to front face rather than back face, and to adopt a thick and suitable strength foam core. Numerical simulations reveal that the increase of front face-sheet thickness led to a remarkable decrease on total energy dissipation while the effect of back face thickness was negligible. The mass allocation strategy with a lighter front face could achieve superior capability in total energy absorption regardless of areal density. Moreover, allocating more mass from back face to foam core is an efficient means to further improve the panel energy absorption.

1. Introduction

The upgradation of ship protection level attracted a great many attentions from the naval departments and related scholars. The potential improvement by optimizing the design of conventional stiffened plate has been exploited sufficiently over a century. Therefore, it becomes impossible to meet the requirements of new weapon threats if the structural weight is limited [1]. The onset of lightweight sandwich structures provides an attractive alternative solution to the problem [2]. Cellular foam core sandwich structures, as a key member in the family of lightweight structures, are of current research and interests due to their high strength-to-weight ratio, stiffness-to-weight ratio and superior energy absorption capability. Especially, the microstructure of foam cores endows them with the ability to undergo large plastic deformation under a relatively long low plateau stress, and thus they could continue to behave excellent blast resistance before collapsing into a more stable state or fracture [3–5].

* Corresponding author. School of Naval Architecture and Ocean Engineering, Huazhong University of Science and Technology, Wuhan, 430074, PR China.

E-mail address: hustlj@hust.edu.cn (J. Liu).

https://doi.org/10.1016/j.marstruc.2019.02.005
Received 12 November 2018; Received in revised form 21 January 2019; Accepted 10 February 2019
Available online 01 March 2019
0951-8339/

Over the past few decades, extensive studies of cellular foam core sandwich structures have been reported on their dynamic responses under impact/blast loadings. Fleck and Deshpande [6] first put forward a three-stage analytical procedure to analyze the blast resistance of clamped sandwich beams, and constructed performance charts for optimizing the geometric parameters to improve the blast resistance for a given mass of sandwich beam. Subsequently, Qiu et al. verified the accuracy of the above theoretical framework by conducting FE calculations [7], and then generalized it to solve the problems of clamped sandwich beams under localized blast loading [8] and clamped circular sandwich plates under uniform blast loading [9]. Tilbrook et al. [10] defined four regimes of behavior by analyzing the relation between the velocity-time curves of front face and back face for sandwich beams under impulsive response, and developed an analytical model to estimate the back face deflection, the degree of core compression and the magnitude of the support reactions. More recently, by incorporating an exact yield criterion considering the effect of core strength into the three-stage model, some theoretical analyses for the dynamic response of sandwich beams [11], panels [12] and shells [13] under blast loadings have been carried out. It indicated that the sandwich structures have superior blast resistance over the equivalent solid plates when the blast intensity is below a critical value [14].

In the experimental aspect, there have appeared some valuable researches on the dynamic response of sandwich structures with foam core under blast loading. The experimental methods used for generating blast loading include metal foam projectile loading technique [15–21], gas gun impact technique (viz. shock tube) [22,23] and the detonation of explosive [14,24–27]. These studies involved in blast events in air and water. The research objects included several types of geometric shape, such as beam [16,18,19], arch [21], panel [17,20] and cylindrical shell [26]. Most attention of these studies was directed towards getting insight into the deformation/failure modes of foam core sandwich structures, and evaluating the superiority of foam core sandwich structures over the monolithic counterparts in terms of blast resistance. In general, several typical failure modes, such as yielding and wrinkling failure of face-sheet, compression and shear failure of core as well as interface failure, have been found. The excellent performance in reducing both the permanent deformation [17] and the peak load of blast wave [25] has been demonstrated.

As expected, numerical investigation into the area of explosion blast response of foam core sandwich structures is of interest to researchers. Hoo fatt et al. [28] examined the through-thickness stress wave response of composite sandwich cylindrical shell under external blast using ABAQUS. It is shown that the blast response of the composite sandwich cylindrical shell would be affected by the magnitude and duration of the pressure pulse. Langdon et al. [27] also got assistance from numerical results in more in-depth understanding of the velocity transfer deformation and dynamic failure mechanisms of sandwich panels comprising with composite face sheets and PVC foam cores. Hassan et al. [29] evaluated the effect of foam density on the blast resistance in terms of failure mode and energy absorption of sandwich panels with PVC foam cores. Liu et al. [30] analyzed the effect of connection condition on the blast resistance of aluminum foam core sandwich panels using LS-DYNA. It was found that poor bonding (disjointed connection) would induce large-scale interfacial delamination and result in undesirable transverse deflection. Jing et al. [31] utilized LS-DYNA to investigate the energy absorption of cylindrical sandwich shells with aluminum foam cores under air blast loading.

Furthermore, in terms of blast performance improvement, there are several potential relevant topics worthy of study on foam core sandwich structures. For example, Qi et al. [32,33] conducted multi-objective optimization of aluminum foam core sandwich structures to seek the optimal configurations, aiming at balancing the energy absorption response and structural deformation response. The blast responses of asymmetric metal sandwich plates were studied experimentally, numerically and theoretically [34–36]. It was found that the impulsive resistance of asymmetric sandwich plates could be enhanced by a reasonable placing sequence of two face-sheets with various face-sheet areal density and material combinations for a given mass. Recently researches indicated that adopting an optimal stepwise graded foam core is a useful means to improve the blast resistance and energy absorption capability of sandwich structures [30,37,38]. The benefit should be attributed to the impedance mismatch between core layers. Another powerful way to improve blast resistance of foam core sandwich structures, could be achieved by combining the advantageous attributes of foam core and prismatic topology core, constructing the so-called hybrid sandwich structures [39–41].

Despite extensive investigations as discussed above on foam core sandwich structures under air blast loading, the great majority of this work concerns the blast performance under low intensity and uniform blast loading where the slapping behavior between panel faces would not be triggered, and detailed elaboration on the deformation/failure mechanisms underlying the overall response is limited. Therefore, the present study aims to further perform combined experimental and numerical investigation into the dynamic response of aluminum foam core sandwich panel under localized air blast loading. A series of experiments were conducted to analyze the effects of face sheet thickness and mass allocation on permanent deflection, deformation/failure modes and associated mechanisms. Finite element simulations were performed to elucidate the deformation and velocity response process, as well as the energy absorption characteristics.

2. Experimental procedure

2.1. Specimen preparation

A schematic of the sandwich specimen with in-plane dimensions of 452 mm (L, length) × 440 mm (B, width) is shown in Fig. 1. It was fabricated from two 304 stainless steel face-sheets bonded to an aluminum foam core using epoxy resin. The mechanical properties of face-sheet base material which were measured by standard quasi-static tests [42], are specified as follows: elastic modulus E = 200 GPa, density ρ = 7900 kg/m^3, yield strength σ_s = 310 MPa, tensile strength σ_p = 740 MPa. Face sheets with different thicknesses (0.54 mm, 0.9 mm, 1.38 mm and 1.8 mm) and foam core with three thicknesses (6 mm, 9 mm and 15 mm) were adopted to assess the effect of key geometric parameters on the blast resistance of sandwich panels under a given blast loading. Of particular interest was that the core density (ρ_c) was of slightly difference for intentional designs in the mass allocation. Specifications

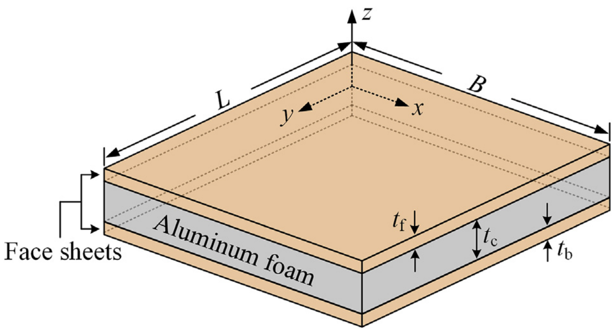

Fig. 1. Schematic of the aluminum foam core sandwich panel.

of the specimens are presented in Table 3.

2.2. Experimental set-up

All the blast tests were conducted in an explosion chamber with an inner diameter of 5 m and a height of 7.5 m. A sketch of the fixture system used for clamping sandwich panels is displayed in Fig. 2. During experiments, the test panels were mounted horizontally and bolted onto a 30 mm thick supporting plate, see Fig. 2(a). A 288 mm × 300 mm square hole was perforated at the center of the supporting plate, providing an open space for the test panels to deform. A 10 mm thick picture frame arranged upon the specimens was used for edge clamping, and left a 288 × 300 mm^2 exposure area to shock wave. As seen from the front view in Fig. 2(b), the supporting platform was connected with I-beam supports along all four edges and then rested on the stiff concrete bricks. The stiff concrete blocks were used to enlarge the cavity space between the supporting plate and foundation to prevent the influence of compressed air on panel deformation response. A rubber pad was set between the I-beam supports and stiff concrete bricks to restrict the movement of apparatus during blast tests. The whole assemblies were roughly located at the bottom center of the explosion chamber. The effect of wall reflection on structural response was thereby negligible. The blast loading was generated by the detonation of a 55 g cylindrical TNT explosive with a radius of 17.5 mm and a height of 37.2 mm, as shown in Fig. 2(d). The charge was placed vertically against the panel center at a certain stand-off distance of 100 mm, measured from center of the explosive to the front face of test panels. It was detonated by an electric detonator slightly buried in the top surface of the explosive. A typical picture of the set-up at the test site just before detonation is shown in Fig. 2(c).

3. Numerical procedure

Three-dimensional finite element calculations were performed using ANSYS/Autodyn to simulate the dynamic response of the aluminum foam core sandwich panels, and to identify the temporal sequence of panel deformations, as well as to get insight into the energy absorption characteristic.

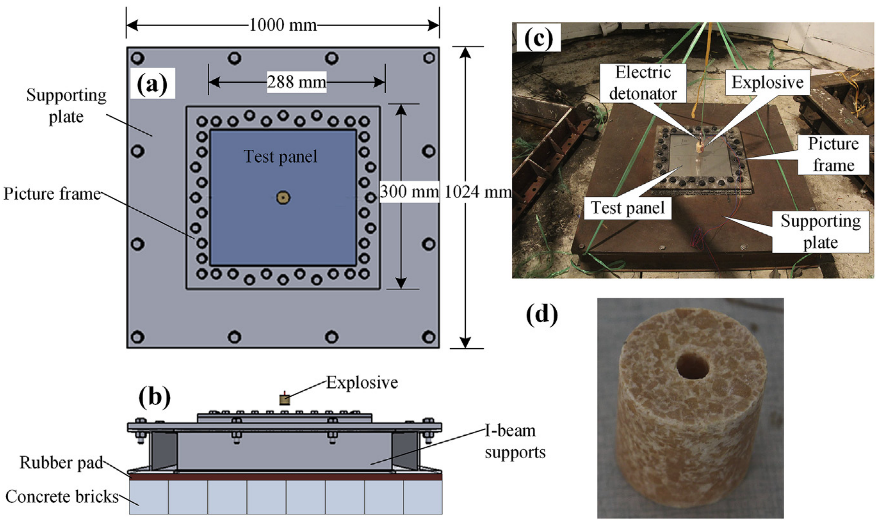

Fig. 2. (a) Top and (b) front views of the schematic of the fixture system used for blast tests; (c) A typical picture of the set-up at the test site just before detonation; (d) Picture of the cylindrical TNT explosive used in experiments.

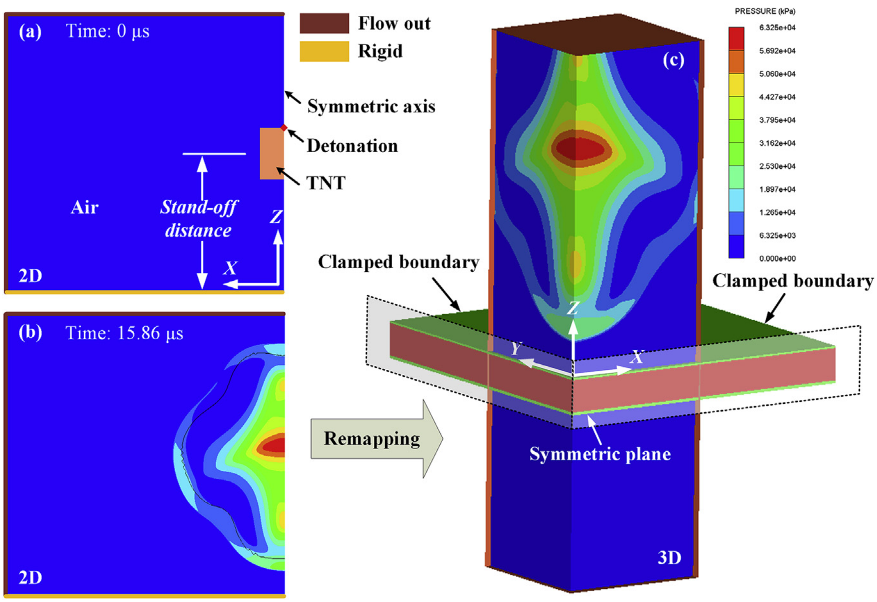

Fig. 3. The result of 2D model remapped into the 3D model. (a) Initial state of 2D model. (b) Pressure contour of 2D model before remapping. (c) Pressure contour of 3D model after remapping.

3.1. Geometry, element, coupling and boundary

The object of study here has an exposure area of 288 × 300 mm^2. Due to the symmetry of the problem, only one quarter of whole sandwich panel within the exposure area was required to be built. According the localization of blast loading, only the central part of the surrounding air media with dimensions of 70 mm × 70 mm × 250 mm was established. Additional studies proved that the proposed scheme of geometric modelling could greatly reduce the computational cost without losing accuracy. Fig. 3(c) shows the numerical model used in the present study.

The face sheets were modelled using Belytschko-Tasy shell element while the explosive and air block were meshed with multi-material Euler elements. The metallic foam core would undergo evident crushing deformation under blast loading, so that if the core was meshed using the Lagrange solids, the elements would become grossly distorted even some remedial action has been taken. Therefore, the solid Arbitrary-Lagrange-Euler (ALE) elements were proposed to model the foam core here. The side length of the shell elements for face sheets was 1.0 mm, while the one of the cubic elements for foam core and air part was also 1.0 mm. Mesh sensitivity studies revealed that further refinement does not significantly improve the accuracy of the calculations. In consideration of the serious debonding failure showing in experiments due to the low strength of adhesive layer, the interactions between face sheets and foam core were treated as automatic surface-to-surface contacts rather than the connection relationship in simulations. The contacts were assumed to be frictionless, and the contact algorithm was formulated using the penalty technique. Importantly, shell parts, including the front face and back face, should be artificially thickened at least twice the largest cell size in the surrounding Euler grid. This procedure would ensure the coupling between shell solver and Eulerian solver function properly [43].

The outer edges of the sandwich panels were modelled as fully clamped to simulate the clamped boundary condition, while the surfaces of the panel located at X = 0 and Y = 0 were set as symmetric boundary. The X = 0 and Y = 0 planes of the fluid domain were also set as symmetric planes, while flow out boundary conditions were applied to four other surfaces to simulate an infinite air field, as shown in Fig. 3(c).

3.2. Blast load modelling

The Euler solvers have the built-in advantage of without having any element distortions during the process of dynamic response. This merit makes the Euler solves well suited for modelling the hydrodynamic behavior, such as explosions. It is known that a very fine mesh is required to ensure the accuracy of ignition, detonation and propagation processes of explosion. The calculation of material flows through cell faces of Euler solves is very time-consuming while adopting a fine mesh. In order to save computational time, the blast load could be modelled in three different stages. Detonation stage: A fine meshed 2D axisymmetric model was firstly established to simulate the ignition, detonation and initial expansion of cylindrical-shaped explosive, as shown in Fig. 3(a). The element length of the 2D model was set to 0.1 mm. In this stage, the panel front face encountered firstly by shock wave was treated as a rigid boundary of Eulerian domain. The 2D model should be run until the shock front gets close to the rigid boundary, as shown in Fig. 3(b). A binary remap file containing the final state of variables of 2D simulations was finally generated. Then, the blast loading modelling got into the loading stage. The results of 2D model are remapped into the 3D Eulerian domain with relative coarse mesh as initial conditions [44], as shown in Fig. 3(c). The explosive could further expand and interact with sandwich panels in the 3D Eulerian

Table 1
Johnson–Cook parameters for 304 stainless steel used in the simulations [45].

Material model parameter	Unit	Value
Yield stress, A	MPa	310
Hardening constant, B	MPa	1000
Hardening exponent, n		0.65
Strain rate constant, c		0.07
Thermal softening exponent, m		1.00
Room temperature, T_r	K	293
Material melting temperature, T_m	K	1673
Ref. strain rate, $\dot{\varepsilon}_0$	s^{-1}	1.00

domain. The particulars of 3D Eulerian domain, including the geometry dimensions, element size, boundary conditions, have been provided in Section 3.1. As the calculation went on, the shock wave would gradually decay. When the pressure of shock was below 300 kPa and the midpoint displacement-time curve of panel began to oscillate around its final value, it meant that the simulation moved into the unloading stage from loading stage. In the unloading stage, the 3D Eulerian domain could be deactivated and the sandwich panel continued to deform freely under its own inertia.

3.3. Material properties

In the numerical model, a Johnson–Cook material model available in ANSYS/Autodyn was employed to model the behavior of base material (304 stainless steel) of panel face sheets. The dynamic flow stress (σ_y) is expressed as the function of strain, strain rate, and temperature:

$$\sigma_y = [A + B(\varepsilon_P^{eq})^n]\left[1 + \ln\left(\frac{\dot{\varepsilon}_P^{eq}}{\dot{\varepsilon}_0}\right)\right]\left[1 - \left(\frac{T - T_r}{T - T_m}\right)^m\right] \tag{1}$$

where ${\varepsilon_p}^{eq}$ is the equivalent plastic strain, $\dot{\varepsilon}_p^{eq}$ is the equivalent plastic strain rate, T is the material temperature, T_m is the material melting temperature and T_r is the room temperature. These constants, including A, B, n, c, m and $\dot{\varepsilon}_0$, are material parameters. The Johnson–Cook parameters for 304 stainless steel are determined from Lee et al. [45], as listed in Table 1. To modified the fracture of the panels, the failure criterion based on equivalent plastic strain was adopted. Note that an element length-dependent failure strain value is critical to capture material failure accurately. In other words, the adopted failure strain value should accommodate to the element size. Considering the element mesh scheme adopted, the failure strain was set to 0.42 according to Ref. [42].

The behavior of aluminum foams with three different densities (i.e., 0.25 g/cm^3,0.33 g/cm^3 and 0.38 g/cm^3) was simulated using the crushable foam model with tension cutoff of 3.31 MPa. The quasi-static compressive stress versus strain curves of the aluminum foams are shown in Fig. 4. The erosion criterion, activated by the instantaneous geometric strain (IGS) limit of 2.0, was applied to remove the grossly distorted elements of foam core. Note that this criterion is a practice widely accepted way and has gained popularity due to its simple and effective formulation [46,47]. The rationality of the setting of IGS limit was also confirmed by comparing the typical results predicted by numerical models with different IGS values. According to the work by Zhang et al. [48], the strain rate effect could be neglected in simulations when the foam density is relatively low.

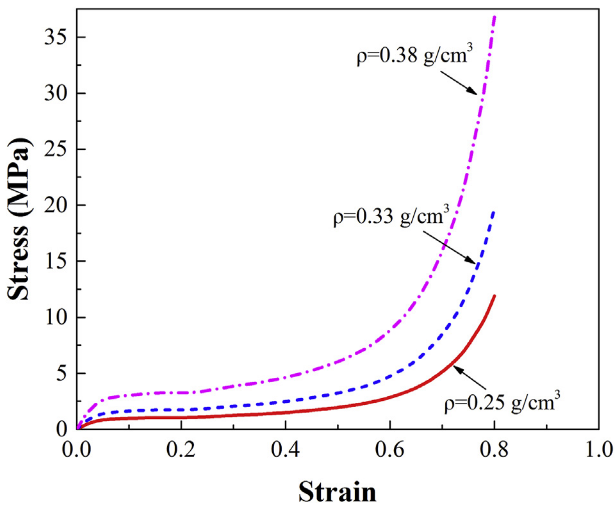

Fig. 4. The measured stress–strain curves of aluminum foam with three different densities under quasi-static compression test.

Table 2
Parameters in Jones-Wilkins-Lee EOS for TNT explosive.

ρ	D	A	B	R_1	R_2	ω	E	V
(kg/m^3)	(m/s^2)	(GPa)	(GPa)				(J/m^3)	
1630	6930	3.712	3.23	4.15	0.95	0.3	7.0×10^9	1.0

The behavior of explosive was typically modelled using the Jones-Wilkins-Lee equation of state [49]. The pressure generated by chemical energy in an explosion can be expressed as follows:

$$P = A\left(1 - \frac{\omega}{R_1 V}\right)e^{-R_1 V} + B\left(1 - \frac{\omega}{R_2 V}\right)e^{-R_2 V}\Bigg) + \frac{\omega E}{V} \tag{2}$$

where P is the hydrostatic pressure, V is the specific volume, E is the specific internal energy and ω, A, B, R_1, and R_2 are material constants, respectively. The values of the constants for TNT explosives have been determined from dynamic experiments and are available in Autodyn [43], as listed in Table 2.

The air and post-burning explosive gas product were assumed to behave as an ideal gas. Hence, the ideal gas equation of state was used for describing the relationship between the pressure and internal energy:

$$P = (\gamma - 1)\rho e \tag{3}$$

where γ is a constant, ρ is air density and e is the specific internal energy. In the simulation, the standard constants of air were adopted from Autodyn material library: $\rho = 1.225 \times 10^{-3}$ g/cm^3 and $\gamma = 1.4$. In order to keep the atmospheric pressure, the air initial internal energy was set as 2.068×10^5 kJ/kg.

4. Experimental results and discussions

The experimental results were classified into two aspects: i) observed deformation/failure modes of the specimens and ii) the midpoint permanent deflections of front and back face sheets.

4.1. Typical deformation/failure modes

Based on the configuration of sandwich panels, the deformation/failure modes of specimens observed in the tests can be classified with respect to the front and back face sheets, as well as foam core, respectively.

4.1.1. Face sheets

The sandwich panels would exhibit the same deformation/failure modes on the face sheets as that of monolithic ones. Menkes and Opat [50] first distinguished the three failure modes of blast-loaded clamped beams: Mode I—large inelastic deformation; Mode II—large inelastic deformation with tensile tearing at the boundary; and Mode III—shearing at the supports. Similar modes were later observed by Teeling-Smith and Nurick [51] for fully clamped circular plates, and Nurick and Shave [52] and Olson et al. [53] for fully clamped rectangular plates. Afterwards, Jacob et al. [54] systematically summarized the failure patterns of blast-loaded plates.

Herein, the failure modes of front (M_f) and back face sheets (M_b) of all tested panels were identified by analyzing their post-

Table 3
Geometric information and experimental results of tested aluminum foam core sandwich panels.

Specimen	Information of sandwich panels					Center deflection		Failure mode	
	t_f	t_b	t_c	ρ_c	ρ_s	δ_f	δ_b	M_f	M_b
	(mm)	(mm)	(mm)	(g/cm^3)	(kg/m^2)	(mm)	(mm)		
AFP-1	0.54	1.38	9.00	0.33	18.14	Failed	39.28	Petalling	I
AFP-2	1.38	1.38	9.00	0.25	24.05	22.62	30.69	I	I
AFP-3	1.80	1.38	9.00	0.33	28.09	18.11	24.02	I	I
AFP-4	0.90	1.80	9.00	0.25	23.58	20.36	29.73	I	I
AFP-5	1.38	1.38	6.00	0.33	23.78	21.59	30.67	I	I
AFP-6	1.38	1.80	6.00	0.33	27.10	18.88	25.71	I	I
AFP-7	1.80	0.90	9.00	0.33	24.30	26.85	27.29	I	I
AFP-8	1.80	1.80	9.00	0.33	31.41	16.67	20.52	I	I
AFP-9	0.90	1.38	15.0	0.38	23.71	23.34	29.25	I	I
AFP-10	1.38	1.38	15.0	0.38	27.50	22.15	23.83	I	I
AFP-11	1.80	1.38	15.0	0.38	30.82	20.15	17.83	I	I
AFP-12	1.80	0.90	15.0	0.38	27.03	21.53	21.06	I	I

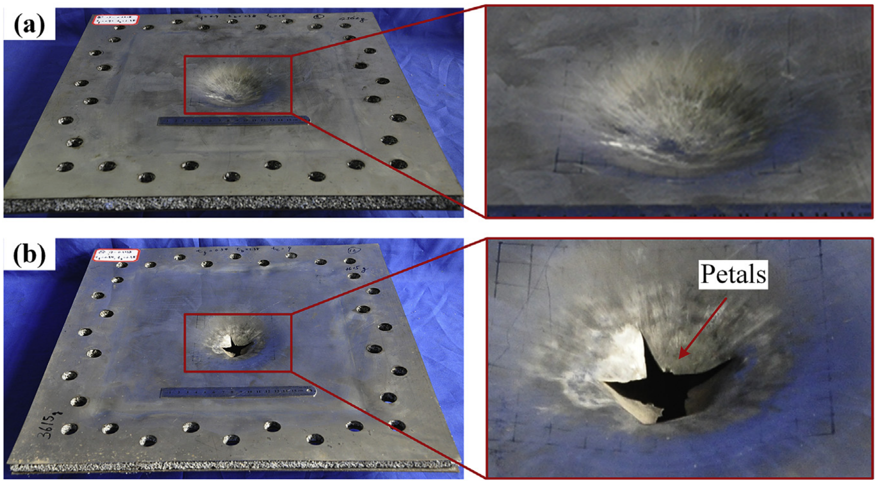

Fig. 5. Photographs showing the typical deformation/failure modes experienced by panel front faces. (a) Large inelastic deformation (Mode I) and (b) Petalling failure mode.

mortem images, as listed in Table 3. Fig. 5 shows the typical post-tested photographs of panel front face sheets with enlarged views. Due to the low stand-off distance, the high temperature and gas products of explosion resulted in a burn phenomenon in the target surface towards blast wave, causing that burn marks could be clearly seen at the center region of front faces. Relative to a large global deformation mode experienced by the panel under far-field explosion, the deformation profile of target front faces was characterized by a small inner dome superimposed atop a large global one when subjected to near-field explosion, as shown in Fig. 5(a). Note that the momentum of the central region of target would be higher than that of the outskirts under this circumstance. The front face with a thin thickness would experience evident indention deformation at the center region, and the principal membrane strains in front face would reach a high level to fracture. Hence, several small petals appeared on the front face of panel **AFP-1**, as presented in Fig. 5(b). In addition, plastic hinges were slightly visible at the four clamped edges of panel front face.

During the blast tests, the back face sheets of all tested panels exhibited large inelastic deformation, referred as Mode I. It can be seen from Fig. 6 that the typical deformation profile of panel **AFP-1** was characterized by a global dome. Relative to the front face sheet, plastic hinges could be obviously observed on the back face skin. A localized pitting also occurred at the top of the dome with a small nose. It was expected that this was due in part to the slapping effect of front face sheet.

4.1.2. Foam core

All the tested specimens were cut into two halves to observe the sectional profiles to understand the core deformation/failure patterns and mechanisms. A typical cross-section view of the post-tested panel **AFP-10** is shown in Fig. 7. Examination of the test results indicated that from the center to outskirts, the entire specimen could be divided into three regions according to the extent of core compression: (1) fully densified region, (2) partially compacted region and (3) non-compacted region, respectively. The fully densified region was located at the central zone of the specimen where the largest plastic deformation occurred. An enlarged view of this area indicated that the cell walls of foam core materials collapsed due to plastic buckling. In the partially compacted region, the compacted pattern was similar but the compression only occurred on the side adjacent to the front face. It meant that the foam core was progressively compressed. A similar phenomenon was found by Theobald et al. [55]. Apart from the crushed damage of foam core, the presence of interface debonding between front face and core layer was highlighted in regions (1) and (2). The compacted-absent region was practically the area clamped by the thick picture frame and thus no effective impulse exerted on this region.

In contrast with panel **AFP-10** (Fig. 7), panel **AFP-1** with a lower core thickness and a thinner front face exhibited a severer failure

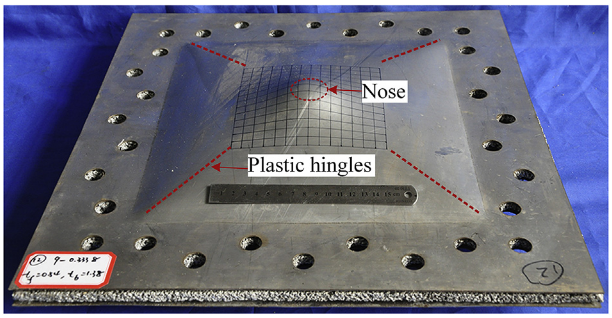

Fig. 6. A photograph showing the typical deformation/failure modes experienced by panel back face.

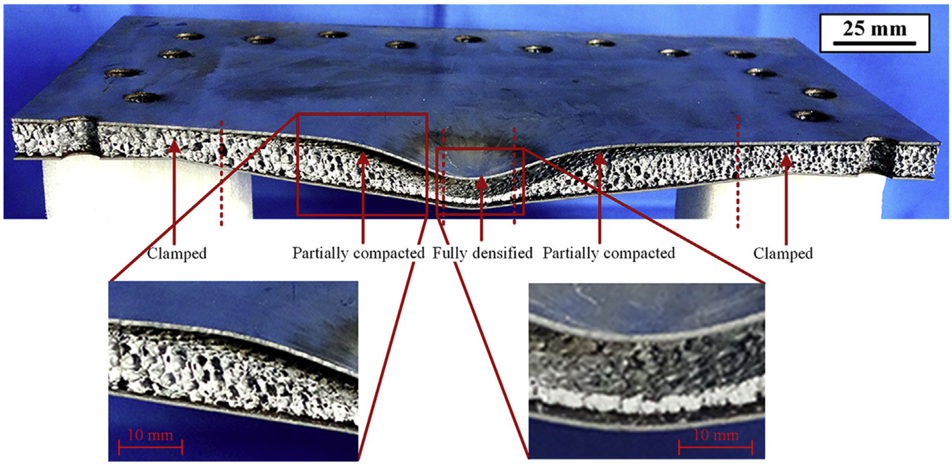

Fig. 7. Cross-section view showing the failure modes of foam core of panel **AFP-10**.

mode in its foam core, as shown in Fig. 8. At the first glance, the foam core material in the center region was found to be disappeared for the reason that the foams were crushed into powder. The extent of core compression in the area from center to outside decreased first and followed by an increasing. Near to the clamped boundary, the core layer underwent a noticeable plastic deformation due to the formation of the plastic hinges of front and back face skins.

It should be noted that debonding failure between face skins and foam core could be found in almost all those tested specimens. It mainly occurred in the center exposed region of sandwich panel while the adhesive strength in the peripheral zone was also affected. It led to the formation of cavity between face sheets and foam core layer. The foam core would be more incapable of accommodating the panel face-sheet deformation once the interface failure appeared, thus influenced the deformation/failure mechanism of sandwich panels.

4.2. Discussions

In this section, by conducting air blast tests, the effects of face-sheet thickness and mass allocation of panel on the dynamic responses of sandwich panels were investigated. The midpoint permanent deflections of front (δ_f) and back (δ_b) face sheets of all tested panels were measured, as summarized in Table 3. Information of the specimen classification for parameter study was given, as listed in Table 4.

4.2.1. Effect of front face-sheet thickness

Herein, the effect of front face-sheet thickness was studied with the panels having same back face-sheet thickness and two kinds of specific core configurations, and tested under the same condition. The effect on the deformation/failure modes is shown in the half sectional views in Fig. 9. When the panels have a thin and low density foam core, the energy dissipation capability of the foam core was so limited that the foam material at the central region was eroded and the front face would slap against back face, see Fig. 9(a)-(c). Under this circumstance, the erosion failure and slapping effect would be aggravated as the decrease of front face-sheet thickness. The front faces of three panels mainly suffered localized dishing deformation. Note that the decrease of front face thickness would

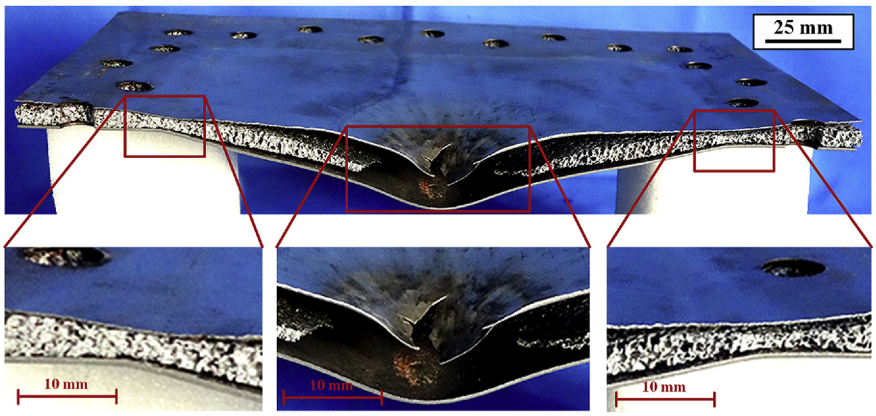

Fig. 8. Cross-section view showing the failure modes of foam core of panel **AFP-1**.

Table 4
Information of the specimen classification for parameter study.

Specimens	Specific configuration	Influence factor
AFP-1, AFP-2, AFP-3	t_b = 1.38 mm, t_c = 9 mm	Front face-sheet thickness
AFP-9, AFP-10, AFP-11	t_b = 1.38 mm, t_c = 15 mm	
AFP-5, AFP-6	t_f = 1.38 mm, t_c = 6 mm	Back face-sheet thickness
AFP-7, AFP-3, AFP-8	t_f = 1.80 mm, t_c = 9 mm	
AFP-12, AFP-11	t_f = 1.80 mm, t_c = 15 mm	
AFP-5, AFP-2, AFP-4, AFP-9	$\rho_s \approx 23.80\ \mathrm{kg/m^2}$	Mass allocation among face sheets and foam core
AFP-6, AFP-10, AFP-12	$\rho_s \approx 27.21\ \mathrm{kg/m^2}$	
AFP-8, AFP-11	$\rho_s \approx 31.12\ \mathrm{kg/m^2}$	

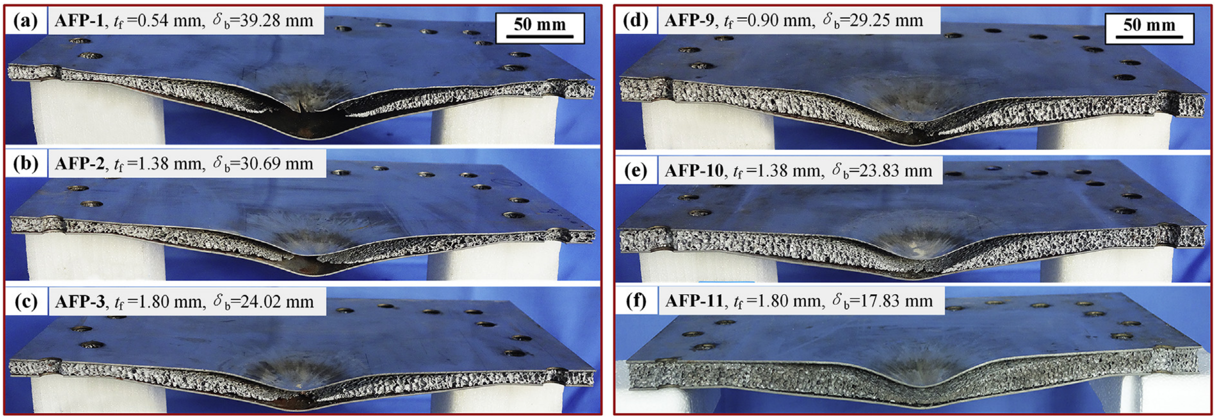

Fig. 9. Cross-section views of sandwich panels with different front face sheet thickness. (a)–(c) t_b = 1.38 mm, t_c = 9 mm; (d)–(f) t_b = 1.38 mm, t_c = 15 mm.

worsen the dishing deformation to reach a high level and even induce petalling failure mechanism. The back faces behaved a smaller inner dome superimposed atop a larger global dome. The inner dome deformation of back face was mainly induced by the slapping effect from front face. The undesirable slapping effect from the decrease of front face sheet resulted in a more noticeable inner dome deformation. If the panels adopted a relatively thick and high density foam core, the panel face sheets would experience large plastic deformation without fracture, as shown in Fig. 9(d)-(f). The thick core provided more space for the deformation of front face sheet. Therefore, the deformation patterns of front faces appeared to be more localized in the central region. As expected, the thinner front face-sheet thickness, the higher front face deformation, and thus the higher impact loading on foam core. Corresponding, the crushing deformation of foam core would be increased. When the thickness of front face sheet was decreased to a low value, the foam material at panel center would be crushed into powder to trigger the slapping behavior. Under this scenario, an inner dome could be found on

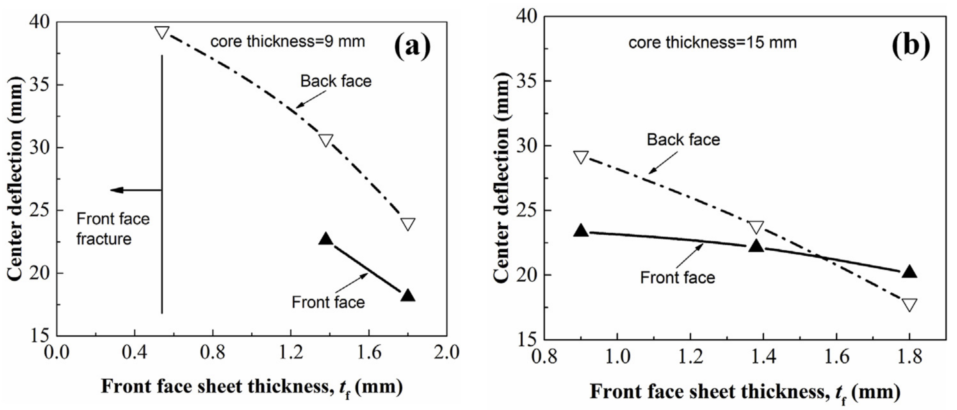

Fig. 10. Effect of front face-sheet thickness on midpoint permanent deflections of front and back face sheets (a) t_b = 1.38 mm, t_c = 9 mm, (b) t_b = 1.38 mm, t_c = 15 mm.

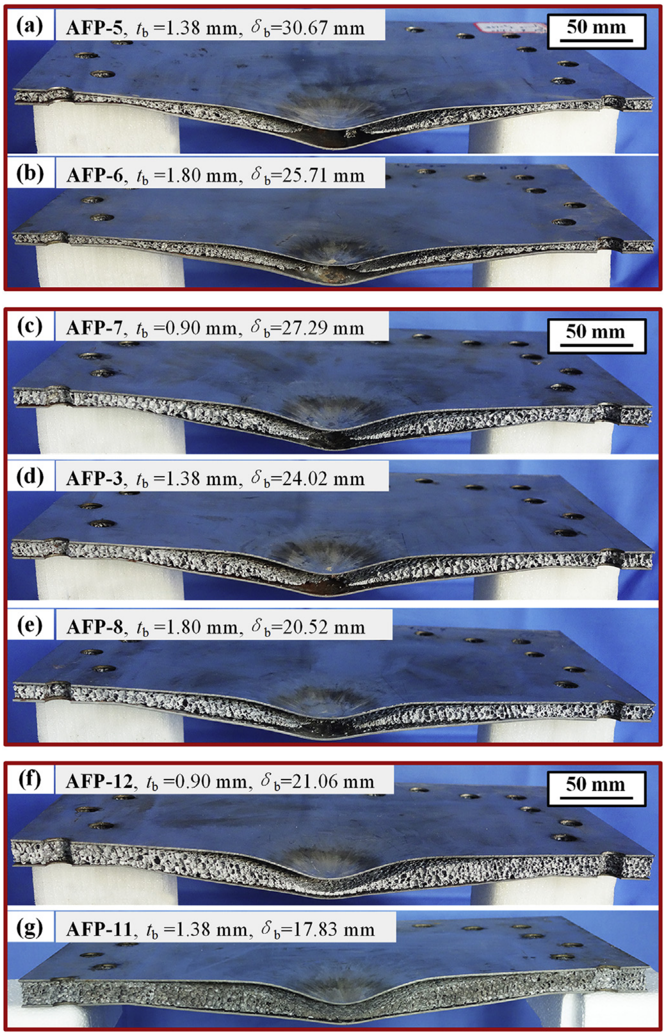

Fig. 11. Cross-section views of sandwich panels with different back face-sheet thickness. (a)–(b) t_f = 1.38 mm, t_c = 6 mm; (c)–(e) t_f = 1.80 mm, t_c = 9 mm; (f)–(g) t_f = 1.80 mm, t_c = 15 mm.

the permanent deformation of back face, as shown in Fig. 9(d).

Fig. 10 shows the effect varying front face-sheet thickness on the midpoint permanent deflections of sandwich panels. Since the panel labeled **AFP-1** with a 0.54 mm thick front face suffered fracture failure on its front face, the value of front face-sheet deflection cannot be measured and thus not included in Fig. 10(a). Obviously the overall permanent deformation kept gradually decreasing as the front face-sheet thickness increases. In present study, the panels with different front face sheet thicknesses in general exhibited a higher back face deflection relative to front face deflection. In addition, the deflection of back face increased more rapidly than that of front face with the decrease of front face thickness, as depicted in Fig. 10(b). The use of foam core with low crush strength should be the root cause of these phenomena. As front face thickness decreased, more foam material would exceed its crush limit and fail into fragment, causing the direct contact between the front and back face. This contact force could inhibit the front face deformation but would also aggravate the back face deformation. In a practical application, this is expected to be hazardous to objects behind the sandwich panel due to the high momentum of back face. It implied that the foam material should have enough thickness and strength to avoid the onset of slapping.

4.2.2. Effect of back face-sheet thickness

In order to comprehensively explore the effect of back face-sheet thickness, the panels were designed to have three specific configurations: 1) medium front face thickness and low core thickness (viz. t_f = 1.38 mm, t_c = 6 mm), 2) high front face thickness and medium core thickness (viz. t_f = 1.80 mm, t_c = 9 mm) and 3) high front face thickness and high core thickness (viz. t_f = 1.80 mm, t_c = 15 mm). The half sections of tested panels are shown in Fig. 11. It can be seen that the effect of back face-sheet thickness on the deformation/failure modes of all panel components was not so evident as that of front face-sheet thickness. It is clear that the panels with different back face-sheet thicknesses exhibited similar deformation modes on their front and back faces. Moreover, not only the

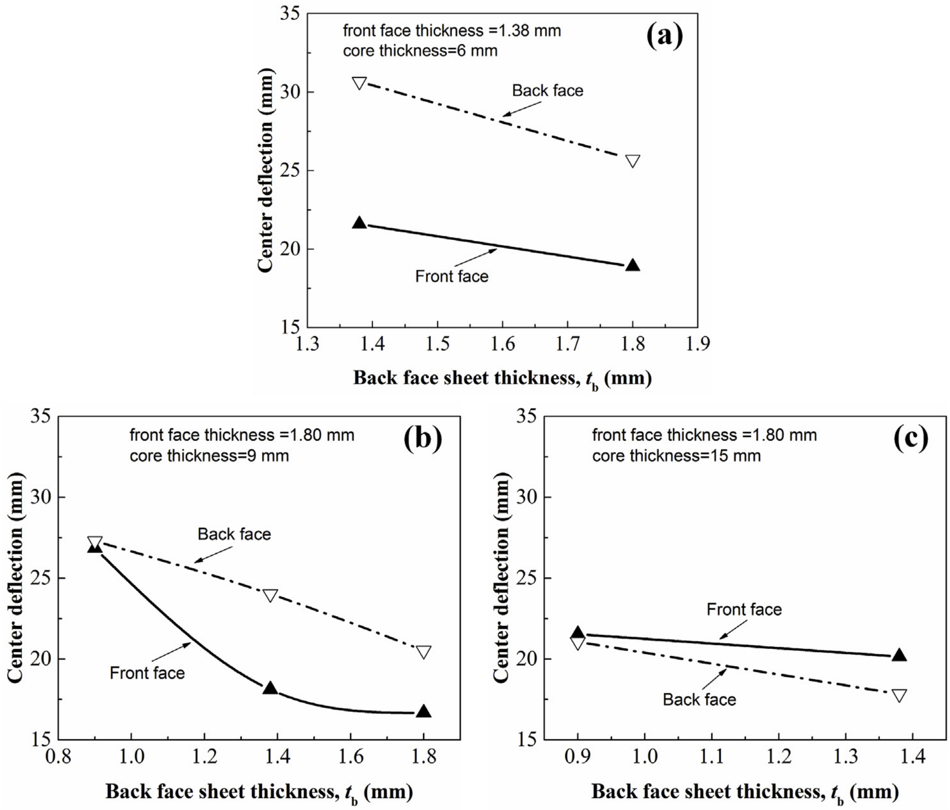

Fig. 12. Effect of back face sheet thickness on the midpoint permanent deflections of face sheets. (a) t_f = 1.38 mm, t_c = 6 mm; (b) t_f = 1.80 mm, t_c = 9 mm; (c) t_f = 1.80 mm, t_c = 15 mm.

fragment failure experienced by foam cores with low or medium thicknesses (see Fig. 11(a)-(e)), but also the crushing deformation underwent by foam cores with high thickness (see Fig. 11(f)-(g)) still existed regardless of back face thickness. Close examination of Fig. 11 shows that with the increase of back face thickness, the global dome shown on front and back faces became shorter.

The measured midpoint deflections of sandwich panels revealed that adopting a thick back face certainly reduced the deformation of front and back faces, as shown in Fig. 12. Moreover, the effect of back face thickness was dependent upon the panel configurations. For the panels with medium front face thickness and low core thickness, the back face thickness had a similar level of influence on the permanent maximum deformation of front and back face, see Fig. 12(a). The back face thickness was not only strongly related to its own flexural rigidity, but also greatly affected the slapping effect between two face sheets. The back face with a similar or higher level of stiffness relative to front face tended to increase the rebound deformation of front face during the slapping process. Under this circumstance, the deformation of back face was always larger than that of front face. If the panel adopted a thick front face and medium core thickness, it still cannot avoid the onset of slapping regardless of the back face thickness considered. But, the back face having small thickness was hard to recoil the front face. Therefore, the difference in deformations of two face sheet was reduced to a low level when the back face is 0.9 mm, as shown in Fig. 12(b). Besides, the effect of back face was similar to that is shown in Fig. 12(a). However, the back face thickness turned out to be a different effect when the panel adopted a thick front face and high core thickness, as plotted in Fig. 12(c). It shows that the back face deformation was more sensitive to the change of back face thickness, and the deformation of back face was no longer larger than that of front face. The onset of the phenomenon should be attributed to the absence of slapping behavior as previously stated.

4.2.3. Effect of mass allocation among face sheets and foam core

Designability is one most attractive feature of sandwich structure, which makes it necessary to study the mass allocation among front face, back face and foam core to optimize the blast performance of foam core sandwich panel. In present study, three groups of panels with different areal density levels were designed to systematically evaluate the effect of mass allocation. The specimens in each group have similar areal density level, and differ in mass allocation among face sheets and foam core. Herein, the areal density levels (denoted as ρ_s) of the specimens in three groups are distributed narrowly around 23.80 kg/m^2 (23.58 kg/m^2 ~ 24.05 kg/m^2), 27.21 kg/m^2 (27.03 kg/m^2 ~ 27.50 kg/m^2) and 31.12 kg/m^2 (30.82 kg/m^2 ~ 31.41 kg/m^2), respectively.

For Group 1 with a specific areal density of round 23.80 kg/m^2, the different mass allocation strategies had a negligible effect on the deformation/failure modes of panel, as shown in Fig. 13(a)-(d). Therefore, the four panels displayed almost the same deformation/failure modes on their components. The profiles of their face sheets resembled a smaller inner dome superimposed atop a

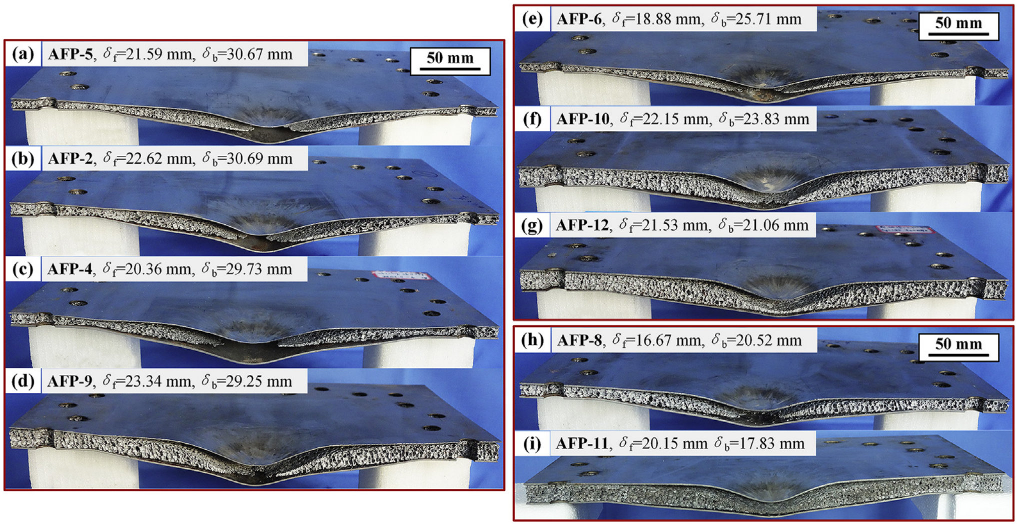

Fig. 13. Cross-section views of sandwich panels with various mass distributions among face sheets and foam core. Group 1 for (a) **AFP-5**; (b) **AFP-2**; (c) **AFP-4**; (d) **AFP-9**; Group 2 for (e) **AFP-6**; (f) **AFP-10**; (g) **AFP-12**; Group 3 for (h) **AFP-8**; (i) **AFP-11**.

larger global dome. All of them experienced severe slapping response and thus the foam material was eroded in relatively large region at the panel center. Actually, there existed a little difference in the erosion region of foam core. Adopting a thin front face and thick back face would aggravate the erosion failure of foam core, as shown in Fig. 13(c). As the areal density level increased to 27.21 kg/m^2 (Group 2) or 31.12 kg/m^2 (Group 3), the effect of mass allocation on the deformation/failure modes seemed to be more noticeable, as shown in Fig. 13(e)-(i). Allocating more mass to front face and foam core could constrain the deformation of front face to prevent it from slapping against back face. Under this circumstance, no erosion failure of foam failure could be found on such panels, and the back face mainly experienced an evident global inelastic deformation, see Fig. 13(g) and (i).

As seen in Fig. 14, the effect of mass allocation on the permanent deformation of the three groups is illustrated using the bar

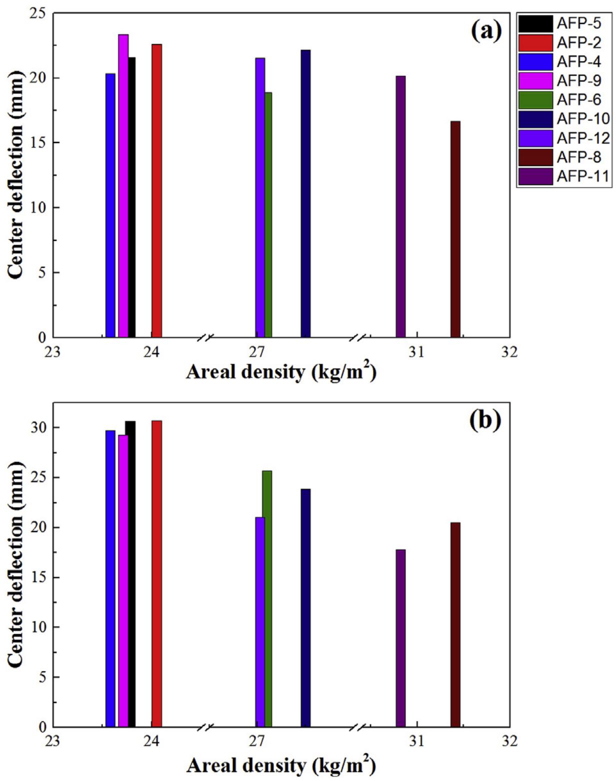

Fig. 14. Effect of mass allocation on the permanent deflections of (a) front face and (b) back face.

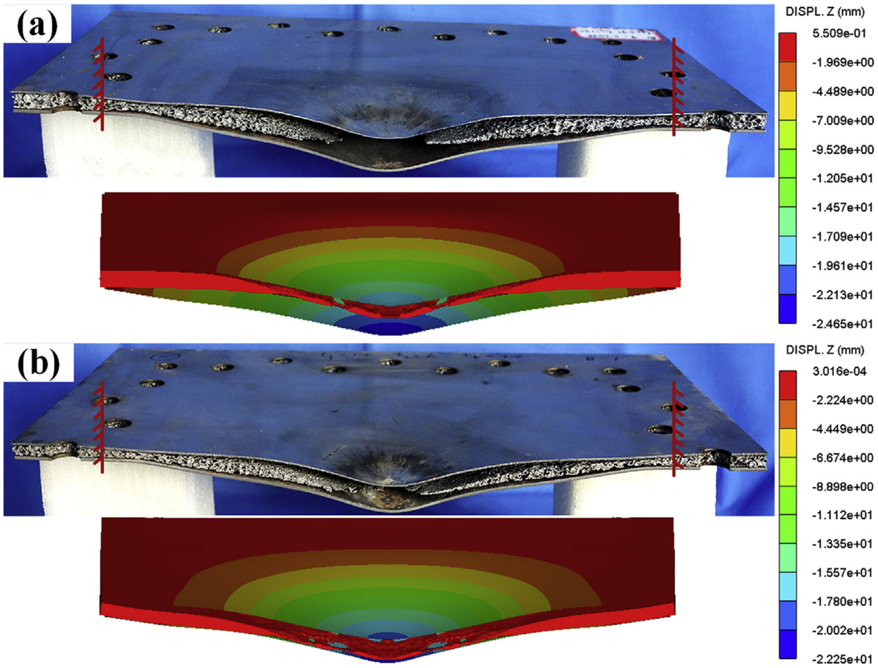

Fig. 15. Comparison of the typical deformation/failure patterns obtained from experiments and simulations. (a) **AFP-4**; (b) **AFP-6**.

diagrams. The relative differences in front and back face deflections are 14.6% and 4.9% for Group 1, 17.3% and 22.1% for Group 2, and 20.9% and 15.1% for Group 3, respectively. It shows that the influence of mass allocation on the back face deformation was very limited when the areal density remained a low level. With the increase of areal density, it would achieve more benefit from the mass allocation to improve the blast resistance. To some extent, there exist contradictory requirements of mass allocation strategies for the deformation reduction of front face and back face. Generally, the back face deflection is considered as the main response of interest from the perspective of the protection of personnel or objects located behind the sandwich panels. Thus, the strategy with a heavy front face, instead of a heavy back face, and the one with a thick and suitable strength foam core should be the optimal solutions for the improvement of protection level in terms of deformation response. This means that the front face has enough flexural rigidity and there is plenty of space for the deformation of front face. The front face and foam core would dissipate shock energy as much as possible through undergoing large plastic deformation. Then, the remaining energy from blast loading transferred to the back face is limited.

5. Numerical results and discussions

The numerical results were analyzed and discussed in terms of the following three aspects: i) validation of numerical model, ii) deformation and velocity responses and iii) energy absorption characteristics.

5.1. Validation of numerical model

The typical contours of deformation/failure patterns obtained from the simulations were compared with the cross sectional views of two typical specimens, as plotted in Fig. 15. It shows that the simulations captured most of the details of failure modes, including the global and localized plastic deformation of face sheets, as well as the fully densified and partially compacted deformation of foam core.

A graph of the predicted midpoint permanent deflections of front and back face sheets versus the experimental values is shown in Fig. 16. It was clear to see that most of the points in Fig. 16 were close to the line of perfect match, indicating a good correlation between the experimental and predicted results. Careful examination revealed that the numerical approach generally underestimated the permanent deflections of back faces. Presumably, this is due to the fact that the erosion failure of foam core predicted by simulations was not as severe as that observed in experiments. Then, the slapping effect would be discounted, so that the momentum gained by back face should be underestimated during the slapping process. According to the results shown above, it is believed that the predictability of the proposed numerical model is reliable in general.

5.2. Deformation and velocity responses

Without loss of generality, two panels (named **AFP-2** and **AFP-12**) were selected to analyze the two typical types of dynamic

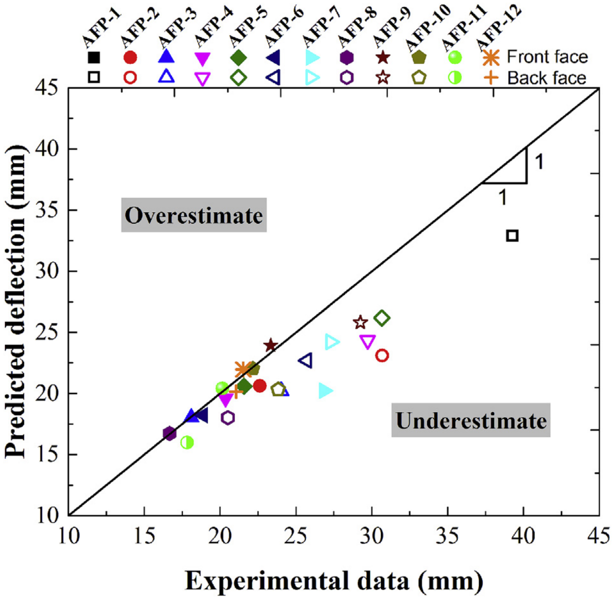

Fig. 16. Numerical versus experimental midpoint permanent deflections of front and back face sheets.

responses in terms of velocity and displacement histories, as shown Fig. 17. As illustrated in Fig. 17(a) for panel **AFP-2** with a core height of 9 mm, the center velocity of front face sheet induced by the blast load quickly reached its peak value at the time of 25 μs and then decreased at a relative slower rate by the core compression. At nearly 31 μs, the center velocity of back face jumped up sharply to its maximum value close to the peak value of front face, while the front face decelerated remarkably. The onset of this phenomenon

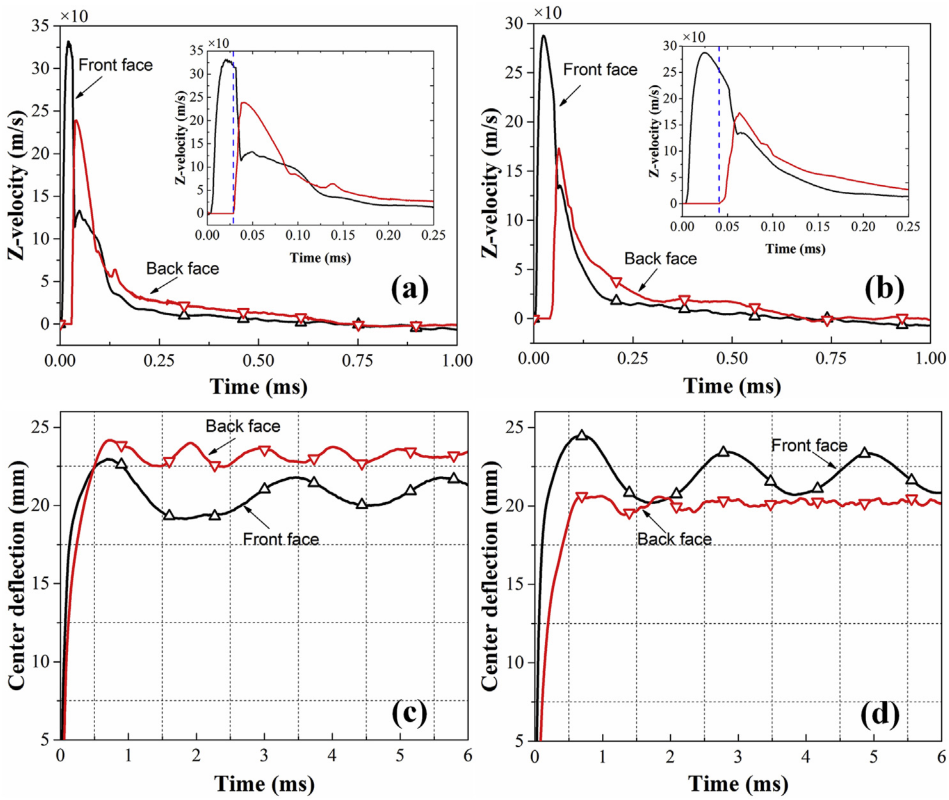

Fig. 17. (a) and (b) show the center velocity and displacement histories of face sheets of panel **AFP-2**, while (c) and (d) present the ones of panel **AFP-12**, respectively.

should be attributed to the fact that the center region of the foam core was totally crushed into densification at this moment, triggering the severe slapping behavior. After that, both front face and back face tended to decelerate gradually to static state through undergoing plastic deformation to dissipate the kinetic energy. However, unlike the perfectly bonded condition, the downward velocities of front and back faces did not achieve a synchronization at the phase of global deformation response because of the interface failure between face sheets and foam core. The center velocity of back face sheet could keep a little higher than that of front face during the kinetic energy dissipation process until the velocities approached zero at 0.8 ms or so. Then, the corresponding midpoint permanent deflection of back face was larger than the that of front face, as plotted in Fig. 17(c). In contrast with **AFP-2**, panel **AFP-12** with a core height of 15 mm presented some different features in velocity and displacement curves of face sheets. It was clear seen from Fig. 17(b) that the back face started to accelerate at a time of around 40 μs lagging behind that of **AFP-2**. Furthermore, the peak value of center velocity for the back face was about one-half of that for front face. Since the foam core in the center resign was just densified but not fragmented according to the photograph damage view shown in Fig. 11(f), the "slapping" effect was drastically diminished while the foam core dissipated considerable impact energy during the compression process. This typical response type was close to Regime B introduced by Tilbrook et al. [10]. Under this circumstance, although the velocity of back face was still larger than that of front face, the deformation response of front face was more evident (see Fig. 17(d)). Careful comparison of the deformation responses shown in Fig. 17(c) and (d) reveals that there existed some difference in oscillation period for the face sheets of two panels. It is known that the oscillation response is associated with the stiffness of object. Therefore, a thick panel face would have a larger oscillation period.

5.3. Energy absorption characteristics

To learn the intrinsic mechanisms of foam core sandwich panels thoroughly, not only the whole process of energy dissipation but also the effects of face-sheet thickness and mass allocation on the energy absorption characteristics were analyzed. The time history curves of plastic energy dissipation of the typical panels named **AFP-2** and **AFP-12** are shown in Fig. 18. The front face, as the first barrier to shock wave, should be the first one to dissipate the shock energy. Then, the foam core and back face would take part in the energy absorption process gradually. Herein, the front face thickness of panel **AFP-2** is relatively thin, and its foam core has a low strength and small height. Once the front face began to deform, the foam core would be compressed easily and the compressed core layer would quickly transfer momentum to back face. Therefore, it can be seen that the energy absorption curves of three components of panel **AFP-2** nearly took off simultaneously, as shown in Fig. 18(a). Due to the excellent compressible property, the foam core dissipated the most energy with the quickest way. The energy dissipation of back face is little bit lower than that of the front face at the initial stage, and finally overtook the latter. By contrast, the panel **AFP-12** with a thick core height offered an available space for front face to deform. The back face won't deform until the front face compressed the thick core to a level enough for generating considerable loading on back face. Therefore, the energy absorption response of back face becomes blunted, as plotted in Fig. 18(b). The front face and foam core dissipated energy with similar level rate, and their contributions on the total energy dissipation reached about 38% and 42%, respectively.

5.3.1. Effect of front face-sheet thickness

Fig. 19 demonstrates the effect of front face thickness on the plastic energy dissipation of each component of sandwich panels with two different front face and core configurations. The scale marks located upon each stack bar were used to quantify the contribution of panel components. The results appeared at the first glance to show that the increase of front face thickness always led to the decrease of total energy absorption regardless of the panel configuration. Close examination of Fig. 19 revealed that only the energy dissipated by front face increased with the increase of its own thickness, and thus the contribution on energy absorption from front face improved by almost 20%. However, the plastic energy dissipation of both the foam core and back face decreased significantly with the increase of front face thickness. This is due to the fact that increasing front face thickness would result in an increase in the stiffness of whole panel. Moreover, the thick front face with high stiffness would also obstruct the momentum transmitted to foam

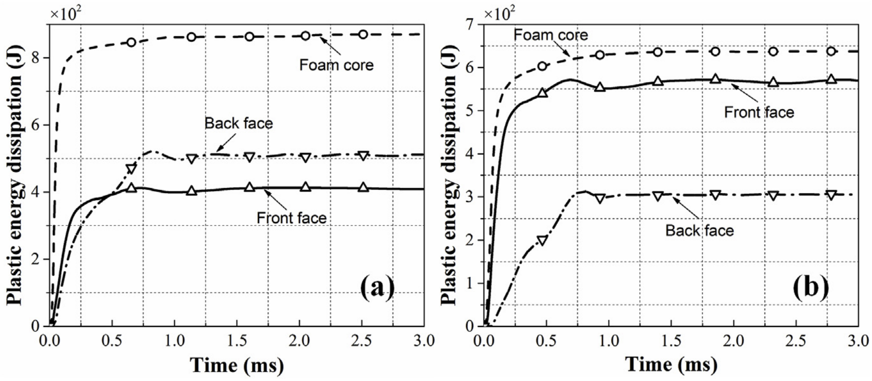

Fig. 18. Typical predicted time history curves of plastic energy dissipation for panels (a) **AFP-2** and (b) **AFP-12**.

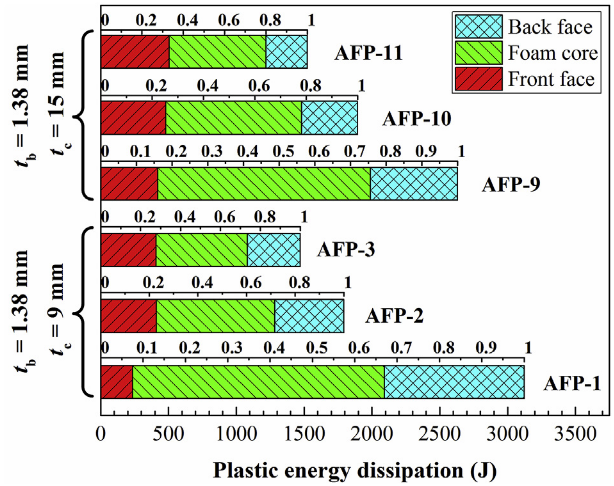

Fig. 19. Effect of front face-sheet thickness on the energy dissipation of each component of sandwich panels.

core. These two factors would yield limited overall deformation of back face and compression of foam core. It can be found that the foam core contributed most to energy absorption regardless of the front face thickness. The role of secondary energy absorber changed from back face to front face with the increase of front face thickness.

5.3.2. Effect of back face-sheet thickness

The effect of back face-sheet thickness on the plastic energy absorption of each component were analyzed for panels with three specific configurations, as plotted in Fig. 20. Generally speaking, the change of back face thickness had negligible influence on the total plastic energy absorption. However, the whole energy would be redistributed among three components. With the increase of back face thickness, the role of foam core was ramped up while the one of front face was diminished, and the back face remained nearly constant. A reasonable understanding of these phenomena should recall the impact of changing the thickness of back face on the shock wave mitigating mechanisms. Obviously, a thick back face would have a high flexural rigidity. From this point of view, the plastic deformation of back face should be limited and thus the corresponding plastic energy dissipation should be reduced. However, a thicker back face tends to provide higher supporting stiffness to foam core, which is beneficial for sufficient crushing deformation of foam core to dissipate more shock energy. Meanwhile, it is believed that a higher stress was transmitted from foam core to back face. The improvement of energy absorption of back face would benefit from this factor. Interestingly, two rival factors for the energy absorption of back face are equal to each other, so that the effect of back face thickness on its own energy absorption was negligible. Besides, the deformation of front face would be restricted due to the high supporting stiffness from back face. This should be the reason why the energy absorption of front face decreased with the increase of back face thickness. The increment in energy absorption from foam core was eroded by the negative effect from front face. Therefore, the back face thickness is hard to affect the total

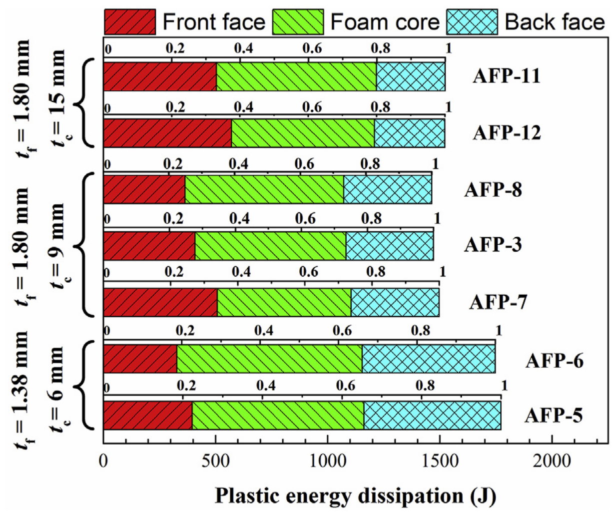

Fig. 20. Effect of back face-sheet thickness on the energy absorption of each component of sandwich panels.

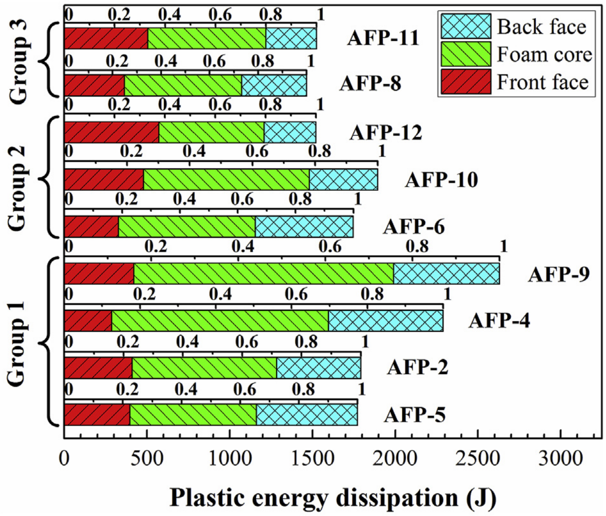

Fig. 21. Effect of mass allocation among face sheets and foam core on energy absorption of each component of sandwich panels.

energy absorption.

5.3.3. Effect of mass allocation among face sheets and foam core

The effect of mass allocation on the energy absorption is much more complicated, as shown in Fig. 21. Obviously, there existed significant difference for three different groups in the effect of mass allocation. But, it cannot be concluded that the effect of mass allocation was strongly related to the level of areal density. Actually, this difference was associated with mass allocation strategies. In Group 1, panels **AFP-5** and **AFP-2** absorbed similar level of shock energy, while panels **AFP-4** and **AFP-9** displayed a higher energy dissipation by 28.9% and 48.4% relative to the former two panels, respectively. Careful examination on the configuration of these four panels shows that allocating less mass to the front face, a common feature of panels **AFP-4** and **AFP-9**, could achieve superior capability in energy absorption. Similarly, this phenomenon also existed in Group 2. Panels **AFP-6** and **AFP-10** with a relatively thin front face dissipated more shock energy than panel **AFP-12**. In addition, the difference in total energy absorption between panel **AFP-8** and panel **AFP-11** was limited due to that they have same front face. The results of energy dissipated by each component of the panels indicated that the mass allocation strategy with a light front face is beneficial for both foam core and back face to dissipate shock energy.

But beyond the strategy associated with front face mass, though, there existed some useful strategies to further improve the energy absorption of panel. Allocating more mass to foam core from back face and increasing the thickness of foam core, panel **AFP-9** dissipated more shock energy than panel **AFP-4** by 14.9%, while panel **AFP-10** and panel **AFP-11** displayed higher energy dissipation than panel **AFP-6** and **AFP-8** by 8.5% and 4.0%, respectively. Note that those strategies are effective means to improve the energy absorption of front face and foam core.

It is worth pointing out that there exists contradiction in requirements of the mass allocation strategies for the minimization of deformation response and for the maximization of energy absorption response. Therefore, seeking a compromised design of foam core panel with satisfactory comprehensive performance is an issue to be addressed in the future.

6. Conclusions

The dynamic response of aluminum foam core sandwich panels under localized air blast loading was investigated by a combination of experiments and simulations in this paper. Main attention is focused on the effects of face-sheet thickness and mass allocation on the blast performance from the aspects of deformation/failure modes, deformation history, energy absorption characteristics and associated mechanisms. Based on the investigations, the following conclusions are drawn:

(1) The aluminum foam core sandwich panels considered here mainly experienced an evident localized deformation superimposed atop a global deformation of front face and a global deformation of back face in response to air blast loading. Besides, the densification and fragment failures of foam core as well as the debonding failure between face skins and foam core appeared to be relatively common occurrence.
(2) The increase of front face thickness would vary the failure mode of front face from petalling failure to large localized inelastic deformation, avoid the onset of inner dome on the deformation profile of back face and ameliorate the fragment failure of foam core to weaken the slapping effect. In contrast, the variation of back face thickness has a limited effect on the deformation/failure modes of panel components.
(3) Although increasing both front face thickness and back face thickness is beneficial to reduce the maximum permanent deflections

of front face and back face, they presented different effect levels on the deformation response. The effect of front face thickness on the back face deflection is relatively notable. Once the slapping behavior occurred, back face thickness would have a similar level of influence on the permanent maximum deformation of two face-sheets; otherwise, a more obvious influence on the back face deformation could be observed.

(4) Effect of mass allocation strategies on deformation/failure modes of panel components is dependent upon the areal density level of panel. The higher the areal density level, the more noticeable the effect. Comparison of permanent deflections indicates that allocating more mass to front face rather than back face and adopting a thick and suitable strength foam core would be the optimal strategies for the reduction of back face deformation.

(5) The plastic energy dissipation of both the foam core and back face was significantly decreased with the increase of front face-sheet thickness, which resulted in a remarkable reduction of total energy absorption. In contrast, the back face thickness marginally affected the total energy absorption. However, with the increase of back face thickness, foam core would dissipate more shock energy and front face would absorb less one.

(6) The mass allocation strategy with a light front face could achieve superior capability in total energy absorption regardless of areal density. Allocating more mass from back face to foam core is an efficient means to further promote the panel energy absorption.

Acknowledgements

The reported research is supported by the National Natural Science Foundation of P.R. China (under the contract numbers of 51509096, 51679098 and 51879112) and the National Research Plan (grant number of JCKY2016206C003). The financial contributions are hereby gratefully acknowledged.

Appendix A. Supplementary data

Supplementary data to this article can be found online at https://doi.org/10.1016/j.marstruc.2019.02.005.

References

[1] Wiernicki CJ, Liem F, Woods GD, et al. Structural analysis methods for lightweight metallic corrugated core sandwich panels subjected to blast loads. Nav Eng J 1991;103(3):192–202.
[2] Liang C-C, Yang M-F, Wu P-W. Optimum design of metallic corrugated core sandwich panels subjected to blast loads. Ocean Eng 2001;28(7):825–61.
[3] Ashby MF, Evans T, Fleck NA, et al. Metal foams: a design guide. Oxford: Butterworth-Heinemann; 2000.
[4] Lu G, Yu T. Energy absorption of structures and materials. Cambridge: Woodhead Publishing Ltd; 2003.
[5] G LJ, A MF. Cellular solids: structure and properties. Cambridge: Cambridge University Press; 1999.
[6] Fleck N, Deshpande V. The resistance of clamped sandwich beams to shock loading. J Appl Mech 2004;71(3):386–401.
[7] Qiu X, Deshpande VS, Fleck NA. Finite element analysis of the dynamic response of clamped sandwich beams subject to shock loading. Eur J Mech A Solid 2003;22(6):801–14.
[8] Qiu X, Deshpande VS, Fleck NA. Impulsive loading of clamped monolithic and sandwich beams over a central patch. J Mech Phys Solid 2005;53(5):1015–46.
[9] Qiu X, Deshpande VS, Fleck NA. Dynamic response of a clamped circular sandwich plate subject to shock loading. J Appl Mech 2004;71(5):637–45.
[10] Tilbrook M, Deshpande V, Fleck N. The impulsive response of sandwich beams: analytical and numerical investigation of regimes of behaviour. J Mech Phys Solid 2006;54(11):2242–80.
[11] Qin QH, Wang TJ. A theoretical analysis of the dynamic response of metallic sandwich beam under impulsive loading. Eur J Mech A Solid 2009;28(5):1014–25.
[12] Qin Q, Yuan C, Zhang J, et al. Large deflection response of rectangular metal sandwich plates subjected to blast loading. Eur J Mech A Solid 2014;47:14–22.
[13] Jing L, Wang Z, Zhao L. An approximate theoretical analysis for clamped cylindrical sandwich shells with metallic foam cores subjected to impulsive loading. Compos B Eng 2014;60:150–7.
[14] Zhu F, Wang Z, Lu G, et al. Some theoretical considerations on the dynamic response of sandwich structures under impulsive loading. Int J Impact Eng 2010;37(6):625–37.
[15] Radford DD, Deshpande VS, Fleck NA. The use of metal foam projectiles to simulate shock loading on a structure. Int J Impact Eng 2005;31(9):1152–71.
[16] Radford DD, Fleck NA, Deshpande VS. The response of clamped sandwich beams subjected to shock loading. Int J Impact Eng 2006;32(6):968–87.
[17] Radford DD, McShane GJ, Deshpande VS, et al. The response of clamped sandwich plates with metallic foam cores to simulated blast loading. Int J Solids Struct 2006;43(7–8):2243–59.
[18] Wang Z, Jing L, Ning J, et al. The structural response of clamped sandwich beams subjected to impact loading. Compos Struct 2011;93(4):1300–8.
[19] Jing L, Wang Z, Ning J, et al. The dynamic response of sandwich beams with open-cell metal foam cores. Compos B Eng 2011;42(1):1–10.
[20] Jing L, Wang Z, Zhao L. The dynamic response of sandwich panels with cellular metal cores to localized impulsive loading. Compos B Eng 2016;94:52–63.
[21] Xie Q, Jing L, Wang Z, et al. Deformation and failure of clamped shallow sandwich arches with foam core subjected to projectile impact. Compos B Eng 2013;44(1):330–8.
[22] Avachat S, Zhou M. High-speed digital imaging and computational modeling of dynamic failure in composite structures subjected to underwater impulsive loads. Int J Impact Eng 2015;77:147–65.
[23] Huang W, Zhang W, Ye N, et al. Dynamic response and failure of PVC foam core metallic sandwich subjected to underwater impulsive loading. Compos B Eng 2016;97:226–38.
[24] Zhu F, Zhao L, Lu G, et al. Structural response and energy absorption of sandwich panels with an aluminium foam core under blast loading. Adv Struct Eng 2008;11(5):525–36.
[25] Liu H, Cao ZK, Yao GC, et al. Performance of aluminum foam–steel panel sandwich composites subjected to blast loading. Mater Des 2013;47:483–8.
[26] Jing L, Wang Z, Shim VPW, et al. An experimental study of the dynamic response of cylindrical sandwich shells with metallic foam cores subjected to blast loading. Int J Impact Eng 2014;71:60–72.
[27] Langdon GS, Karagiozova D, von Klemperer CJ, et al. The air-blast response of sandwich panels with composite face sheets and polymer foam cores: experiments and predictions. Int J Impact Eng 2013;54:64–82.
[28] Hoo Fatt MS, Surabhi H. Blast resistance and energy absorption of foam-core cylindrical sandwich shells under external blast. Compos Struct 2012;94(11):3174–85.
[29] Hassan MZ, Guan ZW, Cantwell WJ, et al. The influence of core density on the blast resistance of foam-based sandwich structures. Int J Impact Eng 2012;50:9–16.
[30] Liu XR, Tian XG, Lu TJ, et al. Sandwich plates with functionally graded metallic foam cores subjected to air blast loading. Int J Mech Sci 2014;84:61–72.

[31] Jing L, Wang Z, Zhao L. Dynamic response of cylindrical sandwich shells with metallic foam cores under blast loading—numerical simulations. Compos Struct 2013;99:213–23.
[32] Qi C, Yang S, Yang L-J, et al. Blast resistance and multi-objective optimization of aluminum foam-cored sandwich panels. Compos Struct 2013;105:45–57.
[33] Qi C, Yang S, Yang LJ, et al. Dynamic response and optimal design of curved metallic sandwich panels under blast loading. Sci World J 2014;2014.
[34] Wang T, Qin Q, Wang M, et al. Blast response of geometrically asymmetric metal honeycomb sandwich plate: experimental and theoretical investigations. Int J Impact Eng 2017;105:24–38.
[35] Wang M, Qin Q, Wang TJ. On physically asymmetric sandwich plates with metal foam core subjected to blast loading: dynamic response and optimal design. Acta Mech 2017;228(9):3265–83.
[36] Yuan C, Qin Q, Wang TJ. A yield criterion for hybrid asymmetric metal sandwich structures and its application. International Journal of Applied Mechanics 2016;08(01):1650001.
[37] Xu F, Zhang X, Zhang H. A review on functionally graded structures and materials for energy absorption. Eng Struct 2018;171:309–25.
[38] Wang E, Gardner N, Shukla A. The blast resistance of sandwich composites with stepwise graded cores. Int J Solids Struct 2009;46(18–19):3492–502.
[39] Vaziri A, Xue Z, Hutchinson JW. Metal sandwich plates with polymer foam-filled cores. J Mech Mater Struct 2006;1(1):97–127.
[40] Zhang P, Cheng Y, Liu J, et al. Experimental study on the dynamic response of foam-filled corrugated core sandwich panels subjected to air blast loading. Compos B Eng 2016;105:67–81.
[41] Cheng Y, Liu M, Zhang P, et al. The effects of foam filling on the dynamic response of metallic corrugated core sandwich panel under air blast loading – experimental investigations. Int J Mech Sci 2018;145:378–88.
[42] Zhang P, Cheng Y, Liu J, et al. Experimental and numerical investigations on laser-welded corrugated-core sandwich panels subjected to air blast loading. Mar Struct 2015;40:225–46.
[43] AUTODYN. Theory manual revision 4.3. Concord: California: Century Dynamics Inc.; 2005.
[44] AUTODYN. Remapping tutorial revision 4.3. Concord: California: Century Dynamics Inc.; 2005.
[45] Lee S, Barthelat F, Hutchinson JW, et al. Dynamic failure of metallic pyramidal truss core materials – experiments and modeling. Int J Plast 2006;22(11):2118–45.
[46] Bandaru AK, Vetiyatil L, Ahmad S. The effect of hybridization on the ballistic impact behavior of hybrid composite armors. Compos B Eng 2015;76:300–19.
[47] Cheng Y, Zhou T, Wang H, et al. Numerical investigation on the dynamic response of foam-filled corrugated core sandwich panels subjected to air blast loading. J Sandw Struct Mater 2017. https://doi.org/10.1177/1099636217700350.
[48] Zhang J, Zhao G, Lu T. Experimental and numerical study on strain rate effects of close-celled aluminum foams. J Xi'an Jiaot Univ 2010;44(5):97–101.
[49] Lee E. JWL equation of state coefficients for high explosives. Lawrence Livermore National Laboratory report; 1973.
[50] Menkes S, Opat H. Tearing and shear failures in explosively loaded clamped beams. Exp Mech 1973;13:480–6.
[51] Teeling-Smith RG, Nurick GN. The deformation and tearing of thin circular plates subjected to impulsive loads. Int J Impact Eng 1991;11(1):77–91.
[52] Nurick GN, Shave GC. The deformation and tearing of thin square plates subjected to impulsive loads—an experimental study. Int J Impact Eng 1996;18(1):99–116.
[53] Olson MD, Nurick GN, Fagnan JR. Deformation and rupture of blast loaded square plates—predictions and experiments. Int J Impact Eng 1993;13(2):279–91.
[54] Jacob N, Nurick GN, Langdon GS. The effect of stand-off distance on the failure of fully clamped circular mild steel plates subjected to blast loads. Eng Struct 2007;29(10):2723–36.
[55] Theobald MD, Langdon GS, Nurick GN, et al. Large inelastic response of unbonded metallic foam and honeycomb core sandwich panels to blast loading. Compos Struct 2010;92(10):2465–75.